1-1-2014

Assessing the time of final deposition of Youngest Toba Tuff deposits in the Middle Son Valley, northern India

Christina M. Neudorf
University of Wollongong, cmn821@uow.edu.au

Richard G. Roberts
University of Wollongong, rgrob@uow.edu.au

Zenobia Jacobs
University of Wollongong, zenobia@uow.edu.au

Assessing the time of final deposition of Youngest Toba Tuff deposits in the Middle Son Valley, northern India

Abstract

We present optical ages for quartz and K-feldspar grains extracted from sedimentary deposits above and below Youngest Toba Tuff (YTT) at two localities in the Middle Son Valley (MSV), Madhya Pradesh, India. These ash deposits have been the focus of past palaeoenvironmental investigations that aim to understand the effects of the ~ 74 ka Toba super-eruption on ecosystems and human populations in northern India. Age estimates from both quartz and feldspar grains post-date the Toba eruption and single-grain age distributions suggest that YTT ash-bearing sediments in the MSV are mainly composed of a mixture of recently sun-exposed, flood-transported grains and older grains from slumped river bank deposits. This study highlights the hazards of using YTT ash as an isochronous marker horizon in the MSV, and illustrates the need to independently assess the time of final deposition of reworked volcanic ash beds in sedimentary sequences used in stratigraphic correlations and palaeoenvironmental reconstructions.

Keywords

Toba eruption, YTT, optical dating, India, palaeoenvironments, archaeology, CAS

Disciplines

Medicine and Health Sciences | Social and Behavioral Sciences

Publication Details

Neudorf, C. M., Roberts, R. G. & Jacobs, Z. (2014). Assessing the time of final deposition of Youngest Toba Tuff deposits in the Middle Son Valley, northern India. Palaeogeography, Palaeoclimatology, Palaeoecology, 399 127-139.

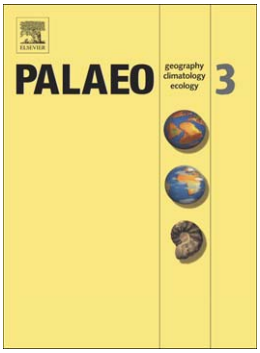

Assessing the time of final deposition of Youngest Toba Tuff deposits in the Middle Son Valley, northern India

C.M. Neudorf, R.G. Roberts, Z. Jacobs

PII: S0031-0182(14)00077-7
DOI: doi: 10.1016/j.palaeo.2014.02.014
Reference: PALAEO 6762

To appear in: *Palaeogeography, Palaeoclimatology, Palaeoecology*

Received date: 9 May 2013
Revised date: 13 November 2013
Accepted date: 10 February 2014

Please cite this article as: Neudorf, C.M., Roberts, R.G., Jacobs, Z., Assessing the time of final deposition of Youngest Toba Tuff deposits in the Middle Son Valley, northern India, *Palaeogeography, Palaeoclimatology, Palaeoecology* (2014), doi: 10.1016/j.palaeo.2014.02.014

Assessing the time of final deposition of Youngest Toba Tuff deposits in the Middle Son Valley, northern India

C. M. Neudorf * [a,b], R. G. Roberts [a], Z. Jacobs [a]

[a] *Centre for Archaeological Science, School of Earth and Environmental Sciences, University of Wollongong, Wollongong, NSW, Australia, 2522*

[b] *Department of Geography, University of the Fraser Valley, Abbotsford, British Columbia, Canada, V2S 7M8*

** Corresponding author, Tel: +1 604-504-7441*

E-mails: C.M. Neudorf (Christina.Neudorf@ufv.ca), R. G. Roberts (rgrob@uow.edu.au), Z. Jacobs (zenobia@uow.edu.au)

ABSTRACT

We present optical ages for quartz and K-feldspar grains extracted from sedimentary deposits above and below Youngest Toba Tuff (YTT) at two localities in the Middle Son Valley (MSV), Madhya Pradesh, India. These ash deposits have been the focus of past palaeoenvironmental investigations that aim to understand the effects of the ~74 ka Toba super-eruption on ecosystems and human populations in northern India. Age estimates from both quartz and feldspar grains post-date the Toba eruption and single-grain age distributions suggest that YTT ash-bearing sediments in the MSV are mainly composed of a mixture of recently sun-exposed, flood-transported grains and older grains from slumped river bank deposits. This study highlights the hazards of using YTT ash as an isochronous marker horizon in the MSV, and illustrates the need to independently assess the time of final deposition of reworked volcanic ash beds in sedimentary sequences used in stratigraphic correlations and palaeoenvironmental reconstructions.

Keywords: Toba eruption, YTT, optical dating, India, palaeoenvironments, archaeology

1. Introduction

Alluvial deposits in the Middle Son Valley (MSV) contain volcanic ash (Youngest Toba Tuff, YTT) and a rich archaeological record in the form of Palaeolithic, Mesolithic and Neolithic artefacts (Sharma and Clark, 1983; Williams et al., 2006) (Fig. 1). The MSV has been the site of archaeological, geological, and palaeoenvironmental investigations that aim to reconstruct regional climate changes in the Late Pleistocene (e.g., Williams et al., 2006), and to understand the effect of the 73.88 ± 0.32 ka Toba volcanic super-eruption (Storey et al., 2012) on ecosystems and human populations in northern India (Jones and Pal, 2005; Williams et al., 2009; Haslam and Petraglia, 2010; Williams et al., 2010). To this end, ash deposits geochemically associated with the YTT (Fig. S1) have been used as chronostratigraphic markers to help correlate the stratigraphies of the Son and neighbouring Belan Valleys (Williams et al., 2006), as well as the Middle Son Basin and the Central Narmada Basin (Acharyya and Basu, 1993). Carbon isotope compositions of pedogenic carbonates sampled above and below the ash in the MSV have been used to infer changes in C_3 and C_4 biomass before and after the Toba eruption (Williams et al., 2009).

The MSV alluvium has been divided into five stratigraphic formations that comprise terraces ranging in height from ~5 m to 35 m above the level of the Son River bed. These formations include (from oldest to youngest) the Sihawal, Khunteli, Patpara, Baghor (lower coarse member, and upper fine member) and Khetaunhi Formations, and are associated with specific Palaeolithic artefact and fossil assemblages (Williams and Royce, 1982; Sharma and Clark, 1983; Williams et al., 2006). Volcanic ash is preserved at two localities: one near the confluence of the Rehi and Son rivers, close to the village of Ghoghara (referred to here as the Ghoghara main section), and one ~25 km downstream (east) of this, on the south bank of the river in the Khunteli Formation type-section (Williams et al., 2006) (Fig. 1).

There are conflicting reports regarding the stratigraphic position of the YTT. Williams and Royce (1982) reported the YTT as part of the coarse member of the Baghor Formation, whereas Williams and Clarke (1995) put the YTT below the Baghor Formation. Jones and Pal (2005) and Jones (2010)

believed the YTT accumulated sometime after deposition of the Patpara Formation, and Williams et al. (2006) reported the YTT as part of a newly discovered formation—the Khunteli Formation—and hypothesized that the Khunteli Formation is actually *older* than the Patpara Formation. Gatti et al. (2011) suggested that these inconsistencies are partly due to an underlying assumption that the stratigraphic position of the YTT ash is laterally continuous and that accumulation of the ash has not been disturbed during vertical accumulation of the valley alluvium. They present a model of river sedimentation in a low-to-medium sinuosity meandering channel that accounts for the laterally discontinuous ash layers observed at both the Ghoghara main section and the Khunteli Formation type-section. The lithostratigraphy of these two ash exposures is described further below.

1.1 Ghoghara main section

The Ghoghara main section is one of eight geological sections near the Rehi-Son confluence that were examined in this study during the 2009 field season and have been described and interpreted by Gatti et al. (2011). The base of all of these sections exposes fining-upward cross-bedded sands and gravels that have been interpreted to represent point-bar or counter-bar formation by a laterally migrating channel, followed by deposition of near-channel overbank sands (Gatti et al., 2011). The overbank sands are overlain by clay that is interpreted to represent a distal, low-energy, shallow-water depositional environment on a floodplain (Gatti et al., 2011). The YTT ash that overlies the clay is thought to have been preserved within a low-energy niche that was later rapidly buried by sediment, such as an oxbow lake or pond on the floodplain (Gatti et al., 2011). Four sites preserving YTT ash, including the Ghoghara main section, are shown in Figure 2. Sedimentological evidence of reworking of the primary ash is present in the form of gradational horizontal contacts and intermixing with the host silt and sand (Fig. 2B), and the fact that the ash-rich units are thicker than ~4–10 cm, which is the expected thickness of primary ash in the region (Gatti and Oppenheimer, 2013).

The Ghoghara main section is a step trench that exposes ~11 m (vertical thickness) of generally fining-upward fluvial gravels, sands and silts, with a white (10YR 8/1, 10YR 8/2) YTT ash-rich unit

appearing between 6 and 7 m below the ground surface (Fig. 1B, Table 1). This ash-rich unit is cohesive and breaks apart in blocks, some of which can still be seen partially buried in colluvium at the foot of the exposure. The lowermost 4 cm of the ash (previously dated by Mark et al., 2013) is exceptionally white (10YR 8/1), contains sharp upper and lower contacts, and is thought to be a primary ash-fall layer (Gatti et al., 2011; Matthews et al., 2012). Biotite crystals from this layer have been $^{40}Ar/^{39}Ar$ dated by Mark et al. (2013) to 72.7 ± 4.1 ka (weighted mean age ± 1σ for 15 multi-grain aliquots) and 95.1 ± 15.3 ka (isochron fit ± 1σ for the same 15 aliquots); both estimates are statistically consistent at 2σ with the astronomically calibrated $^{40}Ar/^{39}Ar$ age of 73.88 ± 0.32 ka for the YTT event (Storey et al., 2012). The ash layer at the Ghoghara main section is the only one to have been dated directly. Its use, therefore, as a time-marker horizon cannot be safely extended to other occurrences of YTT ash in the MSV, or further afield, without independent verification that the ash is *in situ* at all locations and has not been reworked since initial deposition.

Each sedimentary unit within the Ghoghara main section has been assigned a lithofacies code using the code scheme of Miall (2006) (Fig. 1), and the description and interpretation of all facies is shown in Table 1. The fining-upward sands and gravels at the base of the sequence (*Sp*) are interpreted to represent dune formation and migration within the river channel under progressively lower energy flow conditions due to lateral migration of the river channel. These sands grade into silty fine-medium sand (*Sm*) and clayey silt (*Fsm*) that likely record overbank deposition followed by low energy deposition of fines in an abandoned channel, pond, or oxbow lake on a floodplain. The ash (*YTT*) and ash-rich silt (*Fma*) are indicative of ash deposition and preservation within the same low-energy waterbody. The overlying, alternating layers of fine and medium silty sand (*Sma*) and silt with pedogenic features (*P*) represent deposition of overbank sands and floodplain silts followed by soil development on the floodplain. The facies analysis of the sediments in the Ghoghara main section is consistent with the interpretations of Gatti et al. (2011).

1.2 Khunteli Formation type-section

A step trench was excavated at the Khunteli Formation type-section that exposes ~20 m (vertical thickness) of fluvial sands, gravels and silts (Fig. 1C, Table 1). The base of the trench exposes crudely bedded gravels (*Gm*) and cross-bedded sands and gravels (*Sp*) that likely record bar and bedform deposition within a channel. These sediments are overlain by ash-rich sandy silts (*Fma*) that were likely deposited under low-energy or waning flood conditions in a distal environment on the floodplain. The YTT ash-rich silt is laterally discontinuous and may have been deposited within a hollow or abandoned channel. No other ash exposures have been found within 100 m either side of this section, or within the cliff exposures on the north side of the Son River directly opposite Khunteli. The ash-rich silt is overlain by cross-bedded sands (*Sp*) that likely record overbank deposition in an environment slightly more proximal to the channel. This sand grades into sandy silt with pedogenic features (*P*) indicative of the deposition of floodplain fines in a distal environment, followed by soil formation. A sand-matrix supported pebble-cobble gravel unit (*Gm*), not previously described by Gatti et al. (2011), caps the sedimentary sequence and this may be the remnant of a former high-energy river channel deposit that records accelerated flow just prior to incision of the MSV alluvium.

1.3 Optical dating

Optical dating (Huntley et al., 1985; Aitken, 1998) is a numerical dating technique that exploits the luminescence properties of minerals (usually quartz or feldspar) to estimate the time since their last exposure to sunlight (e.g., the time of sediment deposition and burial). Naturally-occurring ionizing radiation in the form of alpha, beta and gamma radiation from the surrounding sediments, and cosmic rays from outer space, causes the redistribution and trapping of electrons in the crystal lattice of buried mineral grains. The calibrated natural OSL or IRSL intensity of a mineral grain—its equivalent dose (D_e)—is used as a measure of the total radiation energy absorbed by that grain since burial. The D_e is combined

with separate measurements of the environmental dose rate at the sampling location to estimate the burial age for the sediment, using the following equation:

Burial age (ka) = equivalent dose (Gy) / environmental dose rate (Gy/ka) (1)

We present optically stimulated luminescence (OSL) ages for single grains of quartz from five samples in the MSV: two collected from below YTT ash, two from above the ash, and one from a modern sandbar in the Son River channel. For these same five samples, we also investigated the potential of K-feldspar (KF) for infrared stimulated luminescence (IRSL) dating using the conventional $IRSL_{50}$ signal (i.e., the IRSL signal measured at 50°C: Wallinga et al., 2000; Blair et al., 2005) and the more recently applied post-infrared IRSL ($pIRIR_{225}$) signal measured at 225°C (after bleaching the sample with infrared photons at 50°C: Thomsen et al., 2008; Buylaert et al., 2009). The latter signal and other elevated temperature pIRIR signals (e.g., Li and Li, 2011) suffer much less than the $IRSL_{50}$ signal from the phenomenon of 'anomalous' (or athermal) fading, which can give rise to substantial KF age underestimates unless an appropriate fading correction is made (e.g., Huntley and Lamothe, 2001). Neudorf et al. (2012) presented single-grain OSL and $IRSL_{50}$ data for one of the below-ash samples (GHO-2) and obtained ages much younger than ~74 ka from both minerals. This unexpected finding prompted the optical dating of additional samples, the results of which are reported here for the first time.

2. Sample collection, preparation and measurement procedures

Two samples for optical dating were collected from above and below the YTT ash at the Ghoghara main section (GHO-2 and GHO-3) and a further pair from the Khunteli type-section (KHUT-1 and KHUT-4) (Fig. 1). A modern sample (KHUT-10) was collected from ~20 cm below the surface of a sand bar in the Son River channel, ~50 m away from the base of the Khunteli type-section, to check for homogeneous bleaching of the OSL, $IRSL_{50}$ and $pIRIR_{225}$ signals in sediments transported recently by the Son River. The sand bar is sufficiently distant from the river banks that it is unlikely to contain older, partially bleached grains derived directly from slumped river bank material. All samples were collected

by hammering steel tubes, ~5 cm in diameter, into the section face, extracting them, and sealing both ends with multiple layers of black plastic. After the tubes had been extracted, the sample holes were widened and a gamma spectrometer detector was inserted for *in situ* gamma ray measurements. Bagged samples of sediment (~60–200 g) were collected from the walls of the gamma spectrometer detector holes for water content measurements, low-level beta counting in the laboratory and high-resolution gamma-ray spectrometry (HRGS). Optical ages were obtained from individual grains of quartz and multi-grain aliquots of KF from all samples associated with the YTT ash, as well as from individual grains of KF from below-ash sample GHO-2.

The equivalent doses were measured using a single-aliquot regenerative (SAR) dose procedure and the environmental dose rates were estimated from field and laboratory measurements of the external beta and gamma contributions, cosmic radiation and the internal dose rate to KF grains (mainly from ^{40}K). Details of the sample preparation and measurement procedures are given in Supplementary Material, together with information on how the environmental dose rates were estimated and the equilibrium status of the ^{238}U and ^{232}Th decay chains as revealed by HRGS.

3. Results

All calculated luminescence ages in this paper should be viewed as estimates of the time since the sediments bracketing the YTT ash were last exposed to sunlight. Ideally, attempts to measure the age of any deposit should entail the application of as many dating techniques as possible; if the results are consistent, then one can conclude that all estimates are likely to approximate the right answer. We first compare the single-grain quartz and single-grain KF results, before considering age estimates for KF multi-grain aliquots obtained from two IRSL signals. This approach is taken because: 1) quartz and feldspar have different luminescence properties and bleaching responses; 2) the experimental conditions used to measure these two minerals differ in many respects (e.g., stimulation sources, preheat temperatures, anomalous fading corrections for KF grains); and 3) the internal dose rates of these minerals differ significantly because of the beta dose rate contribution from ^{40}K inside KF grains.

3.1 Single-grain quartz age estimates

Single-grain quartz OSL ages for all samples are listed in Table 2 and their associated age distributions are plotted in Figures 3A–D. In this paper, the quartz data are shown as age distributions instead of D_e distributions, which are typically reported for quartz, so that they can be directly compared to the fading-corrected age distributions for KF aliquots (see discussion below). The quartz single-grain ages for samples GHO-2, GHO-3, KHUT-1 and KHUT-4 range from less than 20 ka to more than 100 ka, and the overdispersion values range from 35 to 45% (Fig. 3). 'Overdispersion' (OD) is the spread in D_e values remaining after all measurement uncertainties have been taken into account (Galbraith et al., 2005; Galbraith and Roberts, 2012). OD values for single-grain and single-aliquot datasets of quartz samples known or thought to have been fully bleached at burial and not affected by post-depositional disturbance (or by differences in beta dose rate among grains buried at the same time) commonly have OD values of ~10–20% (Galbraith et al., 2005; Jacobs and Roberts, 2007; Arnold and Roberts, 2009). The relatively high OD values for the samples in this study may be the result of: 1) differences in beta dose received by individual grains in their burial environment due to proximity to pore water, calcium carbonate nodules or organic matter (e.g., Lian et al., 1995; Murray and Roberts, 1997; Lian and Huntley, 1999); 2) insufficient or heterogeneous exposure of some grains to sunlight before burial (e.g., Olley et al., 1999, 2004; Arnold et al., 2009); and/or 3) post-depositional intrusion/mixing of younger grains into older deposits or vice versa (e.g., Roberts et al., 1998, 1999; Jacobs et al., 2008). We consider these three potential contributions to the OD below. Grains with unsuitable OSL characteristics were rejected using well-established and objective criteria (Jacobs et al., 2006) and are assumed to contribute little to the OD values reported here.

The sampled sand units above and below the YTT ash (Fig. 1) are non-cohesive, medium-coarse sands that drain freely, contain few carbonate nodules and little organic matter, so pore water, carbonates and organic matter can be ruled out as major contributors to the observed dispersion in the quartz ages. Biswas et al. (2013) also measured 4 quartz samples collected from sedimentary sequences at Ghoghara

(Rehi in their paper) and Khunteli and reported single-grain OD values of 33–45%, which they attributed to beta dose heterogeneity due to spatial variations in ^{40}K concentration. For our samples, some of the spread in single-grain OSL ages may also be due to grain-to-grain differences in beta dose rates from ^{40}K, but it cannot explain all of the observed OD using the ^{40}K values in Table S7 and the model proposed by Mayya et al. (2006). The latter assumes that ^{40}K 'hotspots' result from KF grains scattered randomly in low abundance among quartz grains, with all grains having a median diameter of 200 μm; these narrow constraints (and others in their model) are not true for our samples, or those of Biswas et al. (2013), but an appropriate model would require detailed information about the mineralogical composition of each sample and the spatial distribution of radioactive elements within it.

OSL measurements of a modern sample (KHUT-10) suggest that quartz grains transported by the Son River can become well bleached before burial (Fig. 4A). The quartz single-grain weighted mean D_e was calculated to be –0.02 ± 0.14 Gy, suggesting that the source traps for the OSL signal had been sufficiently emptied by sunlight before burial in most quartz grains. This implies that other transport and depositional processes may be required to explain the high OD values in our ancient samples.

The geomorphic and sedimentary context of our sites suggests that sediment mixing is primarily responsible for the dispersion of single-grain OSL ages in our samples, and perhaps also those reported by Biswas et al. (2013) who did not address this possibility. Mixing may have occurred between pre-existing (pre-Toba) river bank deposits, which have been periodically eroded during floods along the Son River, and younger flood-transported grains. In the MSV, the monsoon season causes the Son River to rise, leading to active erosion of the river banks. Slumped river bank deposits are frequently washed into the channel by rising waters (S. C. Jones 2011, pers. comm.) (Fig. 5). The sampled fluvial, overbank and floodplain sediments in the Ghoghara and Khunteli sedimentary sequences may have been deposited close enough to the river banks to receive a significant contribution of sediment from older deposits. If these older deposits were not transported a significant distance (e.g., river bank sediments that slumped into the channel only a short distance upstream of the sampled sections), then they may have been bleached incompletely before re-deposition, adding scatter to single-grain age distributions.

Using the Finite Mixture Model (FMM) described by Roberts et al. (2000) and Galbraith and Roberts (2012), one can estimate the fewest number of discrete components needed to fit any distribution of mixed-age grains in sediment mixtures. The FMM has been tested using synthetic mixtures of laboratory-dosed grains combined in known proportions (Roberts et al., 2000; Jacobs et al., 2006), and can be used to estimate the number of components in a distribution, as well as their age, for any specified OD. Here, the FMM was applied to the single-grain quartz age distributions following the approach of David et al. (2007) and Jacobs et al. (2008), where the optimal number of components for each sample, the age of each component and the proportion of grains in each component were determined using the maximum log likelihood and Bayes Information Criterion (Galbraith and Roberts, 2012). The optimum number of components and OD value for each component were based on the largest maximum log likelihood value and the smallest Bayes Information Criterion following Jacobs et al. (2008). Each quartz age distribution was best fitted by three components using OD values of between 10 and 20% (Figs 3A–D). The ages of these components, and the proportion of grains represented by each component, are listed in Table 2.

The ages of the components represented by the largest proportion of grains in samples GHO-3, GHO-2, KHUT-4 and KHUT-1 are ~44, ~36, ~43 and ~39 ka, respectively; these are the second oldest components in each of the samples. The oldest components in GHO-2, GHO-3 and KHUT-4 have ages statistically consistent (at 1σ) with the time of the Toba event, whereas the oldest component in KHUT-1 is slightly younger (~62 ka). Overall, the vast majority of quartz grains from all samples appear to be younger than 74 ka, with the FMM component ages indicating that 75–97% were last exposed to sunlight sometime between ~30 and ~70 ka. A minor component (15% of grains or less) of younger FMM ages may reflect the presence of intrusive grains that have been emplaced by plant roots penetrating the cliff face.

If the youngest FMM components indicate the presence of intrusive grains (emplaced by plant roots), then the quartz OSL ages associated with the main FMM components suggest that final deposition

of the sand units bracketing the YTT ash at the Ghoghara main section and the Khunteli type-section occurred sometime between ~36 and ~44 ka (Table 2).

3.2 Single-grain KF age estimates

Neudorf et al. (2012) obtained D_e values for 952 individual feldspar grains (180-212 μm) from a KF-rich extract from sample GHO-2. Fading tests were conducted on all grains and the age estimate of each grain was corrected for its own measured fading rate using the model of Huntley and Lamothe (2001). Measured fading rate uncertainties have been propagated through to the KF grain age uncertainties. Full details on fading test procedures can be found in Neudorf et al. (2012) and are summarised in the Supplementary Material of this article. Fading-corrected $IRSL_{50}$ ages could be determined for 467 of these grains, and the age distribution is reproduced here in Figure 3E.

As with the quartz single-grain distribution, the spread in KF single-grain ages in sample GHO-2 is thought to be mainly due to mixing of potentially well-bleached, fluvially transported sediments with older grains derived from slumping of river bank deposits sometime after the YTT event (Neudorf et al., 2012). Other potential sources of spread, such as grain-to-grain variations in fading rates and internal ^{40}K contents appear to contribute little to the KF single-grain OD (Neudorf et al., 2012), and $IRSL_{50}$ D_e estimates from KF grains collected from the modern sample (KHUT-10) suggest that KF grains transported in the Son River can be well bleached (Fig. 4B). The KF grain age distribution is overdispersed by 37.3 ± 1.5%, which is similar to the OD values obtained for the single-grain OSL age distributions of the four quartz samples (Figs 3A–D). This outcome argues against external ^{40}K hotspots being chiefly responsible for the spread in quartz single-grain OSL ages, as KF grains have a substantial internal dose rate that dilutes the influence of any external variations in beta dose rate.

Like the quartz distribution, the KF single-grain age distribution of GHO-2 is also best fitted with three components using the FMM. Components 1 and 2 are similar in age to those of the quartz distribution, giving us confidence in our single-grain dating procedures. Seventeen percent of the grains constitute a 16 ± 1 ka component, 52% constitute a 30 ± 1 ka component, and 31% of the grains constitute

a 45 ± 2 ka component (Fig. 3E). However, the oldest FMM age component (~45 ka) is noticeably younger than that of the quartz age distribution of the same sample (~70 ka) (compare Figs 3A and E), while the youngest component (~16 ka) is similar in age to that of the quartz distribution (~12 ka), but contains a higher proportion of grains (~17% versus ~3%). Approximately 11% of the single-grain KF ages in the GHO-2 distribution are consistent (at 2σ) with the time of the YTT event, but these were too few in number to be identified as a discrete age component by the FMM.

The reason for the absence of a ~70 ka component in the KF age distribution is unclear. Feathers and Tunnicliffe (2011) measured individual KF grains from a series of samples from southwestern British Columbia, Canada, and noted that some of the oldest grains from each sample were rejected because the natural signal did not intersect the dose-response curve. Of the 1149 KF grains measured for sample GHO-2, only two were rejected as a result of the natural signal failing to intersect the dose-response curve, so this does not explain the apparent paucity of 'old' grains in the KF age distribution. Another possibility is that the ~70 ka quartz grain population was derived from a sediment layer that contained few KF grains. Because KF grains are more susceptible to weathering than quartz (Nesbitt et al., 1997), sufficiently old sediment units in the MSV may contain a paucity of KF grains relative to quartz grains. A further possibility is that quartz grains with OSL ages of ~70 ka were situated closest to KF grains and were thus exposed to above-average beta dose rates during the period of burial from elevated levels of ^{40}K. The samples with the highest ^{40}K concentrations (GHO-2, GHO-3 and KHUT-1; see Table S7) also have the highest proportion of quartz grains in the ~70 ka component (~40%; see Table 2), so there is some support for this proposition. If a beta-dose correction is made to the environmental dose rate for these grains, then their calculated OSL ages will be younger and no longer statistically consistent with the time of the Toba eruption. In summary, the majority of KF grains in sample GHO-2 appear to have been exposed to sunlight sometime after the YTT event, and the same is true also for the quartz grains.

Mark et al. (2013) obtained ^{40}Ar/^{39}Ar ages of between ~42 and ~100 ka for 15 multi-grain aliquots of biotite recovered from the lowermost 4 cm of ash at the Ghoghara main section. The weighted mean age of ~73 ka prompted the authors to remark that "The OSL ages [for GHO-2] are apparently

erroneous and claims that grains have been 'mixed in slump deposits' find no stratigraphic support." However, their comment represents a misreading of the sedimentary processes described by Neudorf et al. (2012), who suggested that sample GHO-2 included some grains derived from older, local riverbank deposits that had slumped into the Son River and were then mixed underwater with younger fluvial sediments transported from upstream. There is no requirement, therefore, for stratigraphic evidence of slumping at the Ghoghara section itself, and we elaborate on this matter further below; some other inaccuracies by Mark et al. (2013) are discussed by Haslam (2013).

3.3 Signal characteristics and bleaching of the $IRSL_{50}$ and $pIRIR_{225}$ signals of small KF aliquots

To confirm our single-grain age estimates, additional age estimates were obtained from small (~3 mm) KF multi-grain aliquots using the $IRSL_{50}$ and $pIRIR_{225}$ signals. Preheat plateau and dose recovery tests suggest that our samples are suitable for $IRSL_{50}$ and $pIRIR_{225}$ SAR procedures; $IRSL_{50}$ and $pIRIR_{225}$ signal characteristics, and preheat plateau and dose recovery test results are discussed in detail in the Supplementary Material.

D_e measurements of quartz and KF grains from KHUT-10 suggest that the OSL and $IRSL_{50}$ signals are bleached more readily in the Son River than the $pIRIR_{225}$ signal (Fig. 4). The weighted mean D_e values from KF aliquots—calculated using the Central Age Model (CAM) of Galbraith et al. (1999)—are 1.3 ± 0.2 Gy (n = 24) and 17.0 ± 2.0 Gy (n = 24) for the $IRSL_{50}$ and $pIRIR_{225}$ signals, respectively (Figs 4C and D). A weighted mean D_e of 1.7 ± 0.2 Gy was obtained by Neudorf et al. (2012) from 366 individual KF grains from sample KHUT-10 using the $IRSL_{50}$ signal (reproduced here as Fig. 4B), which is consistent with multi-grain aliquot estimate.

Average residual doses were also measured for multi-grain aliquots of sample GHO-3 after bleaching them in unfiltered sunlight for 2 days. These are 0.62 ± 0.05 Gy and 5.51 ± 0.43 Gy for the

$IRSL_{50}$ and $pIRIR_{225}$ signals, respectively (see Supplementary Material). These residual doses are considerably smaller than the D_e values for KHUT-10, which was bleached under natural conditions. In addition, variability in the residual doses among sun-bleached aliquots of GHO-3 is also much less than among natural aliquots of KHUT-10, spanning a range of <1 Gy for the $IRSL_{50}$ signal and ~3 Gy for the $pIRIR_{225}$ signal (Fig. S2G). For KHUT-10, there is a ~7 Gy difference between the largest and smallest D_e values for the $IRSL_{50}$ signal (Fig. 4C) and a ~75 Gy range for the $pIRIR_{225}$ signal, which yielded D_e values as high as ~81 Gy (Fig. 4D). These differences are reflected in the OD values for the dose distributions: 18 ± 6% ($IRSL_{50}$) and 19 ± 6% ($pIRIR_{225}$) for GHO-3, compared to the respective values of 92 ± 13% and 64 ± 9% for KHUT-10.

The order-of-magnitude differences between the average residual doses, and the aliquot-to-aliquot variability in residual doses, for GHO-3 and KHUT-10 supports previous reports that the $pIRIR_{225}$ signal is much less light-sensitive than the $IRSL_{50}$ signal (Buylaert et al. 2011; Lowick et al, 2012). It also reinforces the findings of Biswas et al. (2013), who bleached one of their Rehi samples using a filtered sunlamp and obtained average residual doses of ~5 and ~23 Gy from the $IRSL_{50}$ and $pIRIR_{300}$ signals. Collectively, these results demonstrate that: 1) not all KF grains are fully bleached in the Son River before burial; 2) an extended sun-bleach is not analogous to the bleaching conditions experienced by grains transported and deposited in nature; and 3) the $pIRIR_{225}$ signal is more likely than the $IRSL_{50}$ signal to yield age overestimates due to insufficient bleaching.

The Minimum Age Model (MAM) of Galbraith et al. (1999) is commonly used to estimate the D_e of the population of well-bleached grains in samples that were not bleached homogeneously before burial (e.g., Olley et al., 2004; Arnold et al., 2009). We used the MAM to estimate the $IRSL_{50}$ and $pIRIR_{225}$ D_e values of the most fully bleached KF grains in KHUT-10. Before fitting the data with the model, we allowed for D_e overdispersion among multi-grain aliquots that had been well-bleached at deposition by adding (in quadrature) OD values of 20% to each of the D_e measurement errors (Galbraith et al., 2005; Galbraith and Roberts, 2012). The value of 20% is the maximum expected and is based on the OD values of the $IRSL_{50}$ and $pIRIR_{225}$ residual dose distributions for sun-bleached aliquots of GHO-3 (Fig. S2G).

The resulting MAM $IRSL_{50}$ and $pIRIR_{225}$ D_e values for KHUT-10 are 0.4 ± 0.1 Gy ($IRSL_{50}$) and 6.6 ± 1.1 Gy ($pIRIR_{225}$), which are concordant with the average $IRSL_{50}$ and $pIRIR_{225}$ residual doses for the sun-bleached aliquots of GHO-3 (0.6 and 5.5 Gy, respectively). Thus, we consider that the MAM estimates of D_e correspond to the residual doses of well-bleached grains and that larger D_e values likely represent incompletely bleached grains. Note that the residual doses measured from GHO-3 or KHUT-10 have not been corrected for fading here.

3.4 $IRSL_{50}$ and $pIRIR_{225}$ KF aliquot age estimates

$IRSL_{50}$ and $pIRIR_{225}$ D_e values have been determined for samples GHO-2, GHO-3, KHUT-1 and KHUT-4 (24 aliquots of each). In all cases, the average recycling ratios are statistically consistent with unity, suggesting that sensitivity changes between consecutive SAR cycles have been corrected for, and the average recuperation values are also acceptably small (2% or less) (Table S2). The D_e value of each aliquot was corrected for its own measured fading rate using the model of Huntley and Lamothe (2001) (Supplementary Material), and residual doses of 0.4 ± 0.1 Gy ($IRSL_{50}$) and 6.6 ± 1.1 Gy ($pIRIR_{225}$) were subtracted from each fading-corrected D_e estimate. The resulting single-aliquot age distributions are shown in Figures 6A–D. The ages determined using the $pIRIR_{225}$ signal fall mostly in the 40–80 ka time interval (and are overdispersed by 3-22%), whereas the majority of the $IRSL_{50}$ ages are 20–40 ka (with OD values of 14–20%). After correcting for anomalous fading, therefore, the $IRSL_{50}$ ages are typically half as old as those determined using the $IRSL_{225}$ signal. On the basis of observations made in the previous section, we attribute this mainly to inadequate bleaching of the $pIRIR_{225}$ source traps.

As discussed above, we interpret the single-grain quartz and KF age distributions as consisting of multiple age components, with the different components reflecting sediment mixing between river-transported sediment and slumped river bank deposits. Such multi-component structures are, however, concealed in single-aliquot data due to grain-averaging effects, so the FMM cannot be used to resolve discrete D_e or age populations in multi-grain data sets (Arnold and Roberts, 2009; Galbraith and Roberts, 2012). In such instances, the time of the most recent bleaching event can be approximated most closely

by fitting the age distribution with the MAM, to obtain an age estimate for the population of youngest grains. Nonetheless, we recognize that that MAM age estimates, even for small aliquots containing only 2–3 grains of K-feldspar, can yield substantial age overestimates (Feathers and Tunnicliffe, 2011).

The MAM was fitted to each of the multi-grain single-aliquot D_e distributions, after adding an OD value of 5% in quadrature to each D_e measurement error as an estimate of the OD present in the age distribution of single aliquots composed of KF grains that had been well-bleached at deposition and then buried for several tens of millennia. We view a value of 5% as a conservative upper limit, since both the $IRSL_{50}$ and $pIRIR_{225}$ signals yielded OD values of 0% in dose recovery tests on sample GHO-3 (see Supplementary Material). The calculated MAM ages for the $IRSL_{50}$ signal fall between the youngest and second youngest quartz OSL age component identified by the FMM (Figs 3A–D, Table 2). We attribute the youngest quartz component to intrusive grains emplaced by plant roots penetrating the cliff face, so the $IRSL_{50}$ MAM ages should be compared to the second youngest FMM component, which contains the majority of quartz grains (52–75%) in each sample. This comparison shows that the $IRSL_{50}$ MAM ages are younger than the single-grain OSL ages by 8–15 ka. It should be borne in mind, however, that the multi-grain KF aliquots will include some younger, intrusive grains that will reduce their measured ages—for example, sample GHO-2 contains 17% of KF grains with single-grain $IRSL_{50}$ ages of ~16 ka (Fig. 3E). In addition, Li et al. (2013) have shown mathematically and experimentally that the simple dose-subtraction method used here can give rise to D_e underestimates of up to 15% (for the samples in their study), but a shortfall of this magnitude cannot explain all of the difference between the $IRSL_{50}$ and OSL ages for the MSV samples. Based on the dose recovery tests performed on KF grains from sample GHO-3 (see Supplementary Material), we would expect the $IRSL_{50}$ and $pIRIR_{225}$ ages for our samples to be underestimated by not more than 1–2 ka as a result of using the dose-subtraction method.

The MAM ages for the $pIRIR_{225}$ signal are within error of those of the main quartz OSL components for the two above-ash samples (GHO-3 and KHUT-4), but they overestimate by ~15 ka the main OSL ages of the two below-ash samples, GHO-2 and KHUT-1 (Table 2). A potential cause of this age overestimation is that samples GHO-2 and KHUT-1 were deposited with much larger residual doses,

possibly as a result of these samples containing a larger proportion of KF grains derived from older river bank deposits that had slumped into the Son River and had been incompletely bleached when re-deposited. This scenario is supported by the fact that these two samples were positioned closest to the level of the Son River, where bank erosion and slumping during floods in the monsoon season is most likely to occur.

Despite these various uncertainties, however, there is one clear outcome: none of the multi-grain single-aliquot MAM ages are as old as the YTT event, even after making corrections for fading. The two below-ash samples have $pIRIR_{225}$ MAM ages of ~52 ka (GHO-2) and ~54 ka (KHUT-1), and the complete age distributions show that only 4 (of 24) aliquots in sample GHO-2, and none in sample KHUT-1, have individual ages compatible with 74 ka (Figs 6A and 6C). One factor that would increase the calculated ages is if the long-term water content over the period of sample burial had been much higher than we have assumed, and this possibility is explored in the following section.

3.5 Influence of water content on calculated ages

Pore water can severely inhibit the absorption of ionizing radiation by sediment grains in nature, because its absorption coefficient is much higher than that of quartz or feldspar (Lian et al., 1995; Aitken, 1998; Lian and Huntley, 1999). Consequently, it is necessary to adjust the 'as measured' environmental dose rates in cases where the sedimentary water content is suspected to have changed significantly during the burial history of the sample. The measured (field) water contents were all less than 3% (GHO-2: 0.3%; GHO-3: 0.9%; KHUT-1: 1.4%; KHUT-4: 2.8%), expressed as the relative mass of water to mass of dry sediment, but we calculated the $IRSL_{50}$ and $pIRIR_{225}$ ages assuming a long-term, time-averaged water content of 5 ± 2% for all samples. This value is slightly greater than the measured water contents, to take into account sample collection during the dry season, the free-draining (not waterlogged) nature of the deposits, and the monsoonal climate of the region which has a wet season that lasts for one quarter of the year. Saturated water contents of ~22% have been measured in the laboratory for similar sediments in the MSV (Haslam et al., 2011), but even if we assume that our samples were saturated for their entire burial

history, the calculated ages increase by only a few millennia (~3-4 ka) (Table 2). Thus, the $IRSL_{50}$ and $pIRIR_{225}$ ages calculated using the saturated water contents are still much younger (by >38 and >13 ka, respectively) than the expected age of ~74 ka for the YTT ash.

4. Implications for the time of final deposition of the YTT ash and previous palaeoenvironmental reconstructions of Toba's impact

All of the quartz and KF ages presented in this study—whether from individual grains of quartz and KF using the OSL and $IRSL_{50}$ signals, respectively, or from multi-grain aliquots of KF using the $IRSL_{50}$ and $IRSL_{225}$ signals—suggest that final deposition of the sediments bracketing the YTT ash at Khunteli and Ghoghara occurred a few tens of thousands of years after the Toba volcanic super-eruption (Table 2). The fact that we obtain post-YTT ages for the below-ash sediments using two different minerals, two IR-stimulated signals in KF, and single grains as well as aliquots composed of ~30 grains, raises important questions about the time of final deposition of these and other deposits—particularly the YTT ash—in the MSV. We offer two possible explanations for our results.

First, the YTT ash at Ghoghara and Khunteli may have been reworked by fluvial processes after its original emplacement ~74 ka ago, and re-deposited as ash-rich, fluvial silts or as mobile, cohesive blocks of ash, several thousand years after the Toba event. This scenario is illustrated schematically in Figs 7A and 7B. In either of these cases, the lower 4 cm of the YTT ash unit at the Ghoghara main section is likely not primary ash, contrary to the suggestions of Gatti et al. (2011), Matthews et al. (2012) and Mark et al. (2013). A second possible explanation is that the YTT ash was deposited soon after the volcanic eruption, but that the underlying sediments have since been eroded and replaced by younger, inset fluvial sediments (Fig. 7C). These scenarios are not mutually exclusive: for example, the inset sediments in Fig. 7C may also contain blocks of primary or reworked Toba ash. YTT ash and ashy silt observed in the field constitutes cohesive sediment units that are underlain by clayey silt and loose sand (Ghoghara) or unconsolidated medium- to coarse-grained sands (Khunteli) (Fig. 1). It is possible that

coarser sediment underlying the YTT ash units has been preferentially eroded and replaced by younger, inset fluvial sediments (Fig. 7C).

It is possible that the ash and ashy silt units observed in this study are remobilized cohesive blocks of sediment that have been eroded from the cliff face and incorporated in younger fluvial sediments in the Son River channel (Fig. 7B). Modern-day processes give credence to this latter possibility, as ash-rich cohesive silt blocks can be seen today partially buried in colluvium and fluvial sediments along the banks of the Son River (Fig. 5). However, aside from some evidence from the gully shown in Figs 2A and B (photo 2), there is a paucity of evidence to support the 'remobilized ash block' hypothesis from these sedimentary exposures. All observed ash units contain horizontal upper and lower contacts, wherever such contacts are visible (Fig. 2B). There are no sedimentological features within the ash units, such as inclined bedding, or sharp irregular contacts with the surrounding sediment that suggest the ash has been remobilized as a cohesive block before deposition. Thus, most field observations are most consistent with the suggestion that the ash has been reworked by fluvial processes and re-deposited as fluvial silts (Fig. 7A), and/or the non-cohesive underlying sediments have been replaced by younger inset fluvial sediments (Fig. 7C).

The single-grain quartz OSL ages suggest that most grains in the alluvial sediments bracketing the ash were last exposed to sunlight sometime between ~30 and ~70 ka. The latter could conservatively be viewed as an upper limit, because if these grains had experienced enhanced beta dose rates from ^{40}K hotspots then their calculated ages would be younger. The OSL age distributions suggest that samples bracketing the YTT ash at Ghoghara and Khunteli are composed of a mixture of recently sun-exposed flood-transported grains and older grains from slumped river bank deposits, with possibly some intrusive grains emplaced by plant roots penetrating the cliff face. The main FMM component in each of the single-grain OSL age distributions corresponds to a depositional age of between ~36 and ~44 ka (Table 2) and the single-grain $IRSL_{50}$ age distribution of sample GHO-2 consists of 31% of KF grains with ages of ~45 ka and a further 52% with ages of ~30 ka (Fig. 4E). The multi-grain MAM ages range from 22–32 ka ($IRSL_{50}$) to 42–54 ka ($pIRIR_{225}$). If we accept these optical ages as reliable estimates of the time of

deposition of the samples in this study, then the ash-bearing units can be tentatively correlated with the lower coarse member of the Baghor Formation or with the uppermost sediments of the Patpara Formation, as defined by the stratigraphic model of Williams et al. (2006).

We note that the post-Toba ages obtained in this study do not necessarily conflict with the $^{40}Ar/^{39}Ar$ age obtained for the basal YTT ash unit at the Ghoghara main section (Mark et al., 2013) or with the OSL and $pIRIR_{300}$ ages reported for sediments collected at Ghoghara (referred to as Rehi in their paper) and Khunteli (Biswas et al., 2013). The biotite crystals chemically characterized as YTT by Matthews et al. (2012) and dated to ~73 ka by Mark et al. (2013) were extracted from the lowermost 4 cm of ash at Ghoghara considered to be a primary air-fall layer by Gatti et al. (2011). Even if we accept that these crystals were erupted by the YTT event, this does not exclude the possibility that they could have been reworked after initial deposition in the MSV, as this would not have affected the chemical composition of the biotite. Biswas et al. (2013) obtained stratigraphically inverted $pIRIR_{300}$ ages of ~100 and ~60 ka for the 'ash layers' at both Ghoghara and Khunteli, which they attributed to the recent downward percolation of radionuclides. However, thorium is geochemically immobile in most terrestrial environments (Olley et al., 1996, 1997) and the potassium associated with KF grains and volcanic glass is intrinsic to the crystal structure. Moreover, the samples dated by Biswas et al. (2013) were collected from 25–200 cm above the base of the ash unit, so they are unlikely to consist entirely of *in situ* air-fall tephra, if such primary ash has indeed been preserved. We interpret the inverted $pIRIR_{300}$ ages of Biswas et al. (2013) as indicating reworking of YTT ash, and speculate that the two lowest samples are closest in age to the Toba eruption because they contain the highest proportion of minerals (e.g., glass, biotite) associated with this event.

Biswas et al. (2013) also reported quartz OSL ages for sediments above and below the YTT ash unit. They dated the overlying sediments at Ghoghara to 40 ± 5 ka—based on the weighted mean of 51 single-grain D_e values—which is compatible with the main FMM component ages of the above-ash samples at Ghoghara (44 ± 3 ka) and Khunteli (43 ± 3 ka). Their weighted mean ages for quartz grains collected from beneath the YTT ash unit at Khunteli (61 ± 7 ka) and Rehi (70 ± 9 ka) are consistent with

our OSL ages for the oldest FMM component (~40% of the grains) in the below-ash samples at Khunteli (62 ± 5 ka) and Ghoghara (70 ± 5 ka), and with their $pIRIR_{300}$ ages for the lowermost ash samples at Khunteli (66 ± 7 ka) and Ghoghara (61 ± 7 ka); the latter should be considered as maximum estimates as they were corrected for fading but not for the residual dose. They also obtained one older age (83 ± 9 ka) for quartz grains underlying the ash at Ghoghara, but we cannot discount the possibility that those below-ash sediments are in primary context as the exact location (geological section) that they sampled is not recorded. Indeed, we consider it highly unlikely that pre-Toba deposits have been reworked along the entire length of the MSV; pockets of *in situ* sediment will likely be preserved in protected locations.

These results have implications for palaeoenvironmental reconstructions that have been made from pedogenic carbonates sampled from sediments above, below and within YTT ash at excavated sections at the Rehi-Son confluence and in the Khunteli Formation type-section (Williams et al., 2009). The carbon isotope compositions of carbonate nodules and root casts were used to determine whether the vegetation growing in the soils was dominantly following the C_4 pathway of photosynthesis, such as grasses that grow in strong sunlight, or the C_3 cycle of carbon fixation, such as trees, shrubs and grasses growing in shaded forests (Williams et al., 2009). Based on this evidence, it was proposed that C_3 forest was replaced by wooded to open C_4 grassland in north-central India after the Toba eruption (Williams et al., 2009).

The optical ages obtained in this study, and those reported previously by Neudorf et al. (2012) and Biswas et al. (2013), suggest that most of the ash-bearing sediments at the Rehi-Son confluence and at the Khunteli Formation type-section were last deposited many millennia after the YTT event—up to several tens of millennia at some of the key locations used for palaeoenvironmental reconstructions. Given the abundant evidence for reworking and re-deposition of sediments and YTT ash in the MSV, it would be hazardous to assume that ash-bearing sediments can be used as an isochronous marker of the YTT event. Remnant pockets of pre-Toba sediment and YTT ash in primary context are likely to be preserved at some sheltered locations, but the depositional ages would need to be established at each site by direct dating. Any soils, pedogenic carbonate nodules, and root casts associated with reworked

deposits would have formed subsequent to the time of final sediment deposition, so they should not be considered reliable proxies of environmental conditions prevailing before and after the Toba eruption in the absence of independent control on the age of the sedimentary deposits from which the carbonates have been sampled and/or the time of formation of the carbonates themselves.

Toba ash has been identified in many alluvial sequences on the Indian subcontinent (Basu et al., 1987; Anonymous, 1989, 1990, 1991; Devdas and Meshram, 1991; Acharyya and Basu, 1993; Tiwari and Bhai, 1997; Petraglia et al., 2007), but few studies provide evidence that the time of deposition of the ash equates to the time of the volcanic eruption in question. One such study examined a rhyolitic volcanic ash bed preserved in an alluvial sequence containing Acheulian artefacts near the village of Bori in the Kukdi Valley, Pune District (Horn et al., 1993). The ash was dated by K-Ar and fission track methods, which suggested it was erupted 0.54–0.64 Ma ago. A thermoluminescence (TL) age of just 23.4 ± 2.4 ka was obtained from glass shards in the ash and this was interpreted to represent secondary reworking of the tephra and optical annealing of its light-sensitive TL signals long after the original eruption (Horn et al., 1993). Re-deposition of the Bori ash has since been confirmed by the $pIRIR_{300}$ age of 27 ± 3 ka obtained by Biswas et al. (2013), who also reported reworking at another ash locality near Bori. These cautionary findings, coupled with the results presented in this study, highlight the importance of resolving the depositional age of volcanic ash deposits before they are used as chronostratigraphic markers in sedimentary sequences.

5. Summary

In this paper, we present new $IRSL_{50}$, $pIRIR_{225}$ and OSL ages that suggest that YTT ash in the MSV was deposited several tens of thousands of years after the YTT volcanic explosion. The geomorphic context of the sample sites, as well as multi-component single-grain OSL and $IRSL_{50}$ age distributions suggest that fluvial sands bracketing the YTT are composed of a mixture of flood-transported grains and grains derived from slumping river bank deposits, together with some intrusive grains from plant roots penetrating the cliff face. Single-grain quartz age components associated with flood-transported grains

range in age from 36–44 ka placing these deposits within the lower portion of the Baghor Formation or the upper portion of the Patpara Formation in the model of alluvial deposition proposed by Williams et al. (2006). If the lowermost 4 cm of the YTT ash unit at Ghoghara is primary ash-fall, as suggested by Gatti et al. (2011), then this would imply that the underlying fluvial sands are inset sediments deposited later, beneath the relatively cohesive YTT ash unit. But we cannot exclude the possibility that the 'primary ash' at Ghoghara is, in fact, YTT ash that has been eroded from some other location and re-deposited.

The $IRSL_{50}$ and $pIRIR_{225}$ signals from KF grains are well-suited to the SAR procedure, however fading-corrected $pIRIR_{225}$ ages are 1.7–2.3 times older than fading-corrected $IRSL_{50}$ ages, even after subtracting an estimate of the residual dose based on measurements of KF grains from a modern sand bar in the Son River. $pIRIR_{225}$ source traps are less easily bleached than those of the $IRSL_{50}$ signal in our samples, and can be associated with residual doses as high as ~81 Gy. We cannot rule out the possibility, therefore, that the residual dose correction applied to the $pIRIR_{225}$ ages is insufficient, and that the calculated ages appear too old due to inadequate bleaching of the sediments during their last episode of subaqueous transport by the Son River.

Previous palaeoenvironmental reconstructions inferred from the carbon isotope composition of pedogenic carbonates sampled below, within and above the YTT ash in the MSV (Williams et al., 2009) should be regarded as potentially compromised. The optical ages presented here suggest that the sediments bracketing the YTT at these locations—and, hence, any pedogenic carbonates preserved in them—were most likely deposited tens of millennia after the ~74 ka Toba event. We recommend that sedimentary sequences containing volcanic ash beds should be more commonly investigated using optical dating methods to assess the final time of deposition of the ash before employing it as a local or regional chronostratigraphic marker.

Acknowledgements

This project was funded by an ARC Discovery Project grant to R.G.R. and University of Wollongong scholarships to C.M.N. We thank S. Huot for advice and Excel macros for fading

corrections, M. Petraglia and J.N. Pal for introducing us to the field sites and for archaeological advice, the local villagers of the MSV for help with field excavations and sampling, and J.-H. May for constructive comments on an earlier version of this manuscript.

References

Acharyya, S. K., Basu, P. K., 1993. Toba ash on the Indian subcontinent and its implication for the correlation of Late Pleistocene alluvium. Quaternary Research 40 (1), 10-19.

Aitken, M. J., 1998. An Introduction to Optical Dating. Oxford University Press, Oxford.

Anonymous, 1989. Late Quaternary ash bed in the Barakar River section, Bihar. News Geological Survey of India, Central Headquarters 20, 18.

Anonymous, 1990. Late Quaternary ash bed and Acheulian implements from Orissa - The implication. News Geological Survey of India, Eastern Region 10, 7.

Anonymous, 1991. Volcanic ash in Quaternary formations Sagileru valley. News Geological Survey of India, Southern Region 9, 9.

Arnold, L. J., Roberts, R. G., 2009. Stochastic modelling of multi-grain equivalent dose (D_e) distributions: implications for OSL dating of sediment mixtures. Quaternary Geochronology 4 (3), 204-230.

Arnold, L. J., Roberts, R. G., Galbraith, R. F., DeLong, S. B., 2009. A revised burial dose estimation procedure for optical dating of young and modern-age sediments. Quaternary Geochronology 4 (4), 306-325.

Basu, P. K., Biswas, S., Acharyya, S. K., 1987. Late Quaternary ash beds from Son and Narmada basins, Madhya Pradesh. Indian Minerals 41, 66-72.

Biswas, R. H., Williams, M. A. J., Raj, R., Juyal, N., Singhvi, A. K., 2013. Methodological studies of luminescence dating of volcanic ashes. Quaternary Geochronology 17, 14-25.

Blair, M. W., Yukihara, E. G., McKeever, S. W. S., 2005. Experiences with single-aliquot OSL procedures using coarse-grain feldspars. Radiation Measurements 39 (4), 361-374.

Buylaert, J. P., Murray, A. S., Thomsen, K. J., Jain, M., 2009. Testing the potential of an elevated temperature IRSL signal from K-feldspar. Radiation Measurements 44 (5-6), 560-565.

Buylaert, J. P., Thiel, C., Murray, A. S., Vandenberghe, D. A. G., Yi, S., Lu, H., 2011. IRSL and post-IR IRSL residual doses recorded in modern dust samples from the Chinese Loess Plateau. Geochronometria 38, 432-440.

David, B., Roberts, R. G., Magee, J., Mialanes, J., Turney, C., Bird, M., White, C., Keith Fifield, L., Tibby, J., 2007. Sediment mixing at Nonda Rock: investigations of stratigraphic integrity at an early archaeological site in northern Australia and implications for the human colonization of the continent. Journal of Quaternary Science 22 (5), 449-479.

Devdas, V., Meshram, S. N., 1991. Search for Quaternary ash bed in the Quaternary basins of Orissa. Records Geological Survey of India 124, 40-42.

Feathers, J., Tunnicliffe, J., 2011. Effect of single-grain versus multi-grain aliquots in determining age for K-feldspars from southwestern British Columbia. Ancient TL 29 (2), 53-58.

Galbraith, R. F., Roberts, R. G., 2012: Statistical aspects of equivalent dose and error calculation and display in OSL dating: An overview and some recommendations. Quaternary Geochronology 11, 1-27.

Galbraith, R. F., Roberts, R. G., Laslett, G. M., Yoshida, H., Olley, J. M., 1999. Optical dating of single and multiple grains of quartz from Jinmium rock shelter, northern Australia: Part I, experimental design and statistical models. Archaeometry 41 (2), 339-364.

Galbraith, R. F., Roberts, R. G., Yoshida, H., 2005. Error variation in OSL palaeodose estimates from single aliquots of quartz: a factorial experiment. Radiation Measurements 39 (3), 289-307.

Gatti, E., Durant, A. J., Gibbard, P. L., Oppenheimer, C., 2011. Youngest Toba Tuff in the Son Valley, India: a weak and discontinuous stratigraphic marker. Quaternary Science Reviews 30, 3925-3934.

Gatti, E., Oppenheimer, C. 2013. Utilization of distal tephra records for understanding climatic and environmental consequences of the Youngest Toba Tuff, in: Giosan, L., Fuller, D. Q., Nicoll, K., Flad, R. K., Clift, P. D. (Eds.), Climates, Landscapes and Civilizations. American Geophysical Union, Washington, D.C., pp. 63-73.

Haslam, M., 2013. Climate effects of the 74 ka Toba Super-eruption: Multiple interpretive errors in 'A high precision $^{40}A/^{39}A$ age for the Young Toba Tuff and dating of ultra-distal tephra' by D. Mark et al.. Quaternary Geochronology In Press, 1-2.

Haslam, M., Petraglia, M., 2010. Comment on "Environmental impact of the 73 ka Toba super-eruption in South Asia" by M.A.J. Williams, S.H. Ambrose, S. van der Kaars, C. Ruehlemann, U. Chattopadhyaya, J. Pal and P.R. Chauhan [Palaeogeography, Palaeoclimatology, Palaeoecology 284 (2009) 295-314]. Palaeogeography, Palaeoclimatology, Palaeoecology 296 (1-2), 199-203.

Haslam, M., Roberts, R. G., Shipton, C., Pal, J. N., Fenwick, J. L., Ditchfield, P., Boivin, N., Dubey, A. K., Gupta, M. C., Petraglia, M., 2011. Late Acheulean hominins at the Marine Isotope Stage 6/5e transition in north-central India. Quaternary Research 75 (3), 670-682.

Horn, P., Müller-Sohnius, D., Storzer, D., Zöller, L., 1993. K-Ar-, fission-track-, and thermoluminescence ages of Quaternary volcanic tuffs and their bearing on Acheulian artifacts from Bori, Kukdi Valley, Pune District, India. Zeitschrift der Deutschen Geologischen Gesellschaft 144, 326-329.

Huntley, D. J., Godfrey-Smith, D. I., Thewalt, M. L. W., 1985. Optical dating of sediments. Nature 313, 105-107.

Huntley, D. J., Lamothe, M., 2001. Ubiquity of anomalous fading in K-feldspars and the measurement and correction for it in optical dating. Canadian Journal of Earth Sciences 38, 1093-1106.

Jacobs, Z., Duller, G. A. T., Wintle, A. G., 2006. Interpretation of single grain D_e distributions and calculation of D_e. Radiation Measurements 41 (3), 264-277.

Jacobs, Z., Roberts, R. G., 2007. Advances in optically stimulated luminescence dating of individual grains of quartz from archaeological deposits. Evolutionary Anthropology 16 (6), 210-223.

Jacobs, Z., Wintle, A. G., Duller, G. A. T., Roberts, R. G., Wadley, L., 2008. New ages for the post-Howiesons Poort, late and final Middle Stone Age at Sibudu, South Africa. Journal of Archaeological Science 35 (7), 1790-1807.

Jones, S. C., 2010. Palaeoenvironmental response to the ~74 ka Toba ash-fall in the Jerreru and Middle Son valleys in southern and north-central India. Quaternary Research 73 (2), 336-350.

Jones, S. C., Pal, J. N., 2005. The Middle Son Valley and the Toba Supervolcanic Eruption of ~74 kyr BP: Youngest Toba Tuff deposits and Palaeolithic associations. Journal of Interdisciplinary Studies in History and Archaeology 2 (1), 47-62.

Li, B., Li, S. –H., 2011. Luminescence dating of K-feldspar from sediments: A protocol without anomalous fading correction. Quaternary Geochronology 6, 468-479.

Li, B., Roberts, R. G., Jacobs, Z., 2013. On the dose-dependency of the bleachable and non-bleachable components of IRSL from K-feldspar: Improved procedures for luminescence dating of Quaternary sediments. Quaternary Geochronology 17, 1-13.

Lian, O. B., Hu, J., Huntley, D. J., Hicock, S. R., 1995. Optical dating studies of Quaternary organic-rich sediments from southwestern British Columbia and northwestern Washington State. Canadian Journal of Earth Sciences 32 (8), 1194-1207.

Lian, O. B., Huntley, D. J., 1999. Optical dating studies of postglacial aeolian deposits from the south-central interior of British Columbia, Canada. Quaternary Science Reviews 18 (13), 1453-1456.

Lowick, S. E., Trauerstein, M., Preusser, F., 2012. Testing the application of post IR-IRSL dating to fine grain waterlain sediments. Quaternary Geochronology 8, 33-40.

Mark, D. F., Petraglia, M., Smith, V. C., Morgan, L. E., Barfod, D. N., Ellis, B. S., Pearce, N. J., Pal, J. N., Korisettar, R., 2013. A high precision $^{40}A/^{39}A$ age for the Young Toba Tuff and dating of ultra-distal tephra: Forcing of Quaternary climate and imlications for hominin occupation of India. Quaternary Geochronology In Press, 1-14.

Matthews, N. E., Smith, V. C., Costa, A., Durant, A. J., Pyle, D. M., Pearce, N. J. G., 2012. Ultra-distal tephra deposits from super-eruptions: Examples from Toba, Indonesia and Taupo Volcanic Zone, New Zealand. Quaternary International 258, 54-79.

Mayya, Y. S., Morthekai, P., Murari, M. K., Singhvi, A. K., 2006. Towards quantifying beta microdosimetric effects in single-grain quartz dose distribution. Radiation Measurements 41, 1032-1039.

Miall, A. D., 2006. The Geology of Fluvial Deposits. Springer, Berlin.

Murray, A. S., Roberts, R. G., 1997. Determining the burial time of single grains of quartz using optically stimulated luminescence. Earth and Planetary Science Letters 152 (1-4), 163-180.

Nesbitt, H. W., Fedo, C. M., Young, G. M., 1997. Quartz and feldspar stability, steady and non-steady state weathering, and petrogenesis of siliciclastic sands and muds. The Journal of Geology 105 (2), 173-192.

Neudorf, C. M., Roberts, R. G., Jacobs, Z., 2012. Sources of overdispersion in a K-rich feldspar sample from north-central India: Insights from D_e, K content and IRSL age distributions for individual grains. Radiation Measurements 47 (11-12), 696-702.

Olley, J. M., Caitcheon, G. G., Roberts, R. G., 1999. The origin of dose distributions in fluvial sediments, and the prospect of dating single grains from fluvial deposits using optically stimulated luminescence. Radiation Measurements 30 (2), 207-217.

Olley, J. M., Murray, A., Roberts, R. G., 1996. The effects of disequilibria in the uranium and thorium decay chains on burial dose rates in fluvial sediments. Quaternary Science Reviews 15 (7), 751-760.

Olley, J. M., Pietsch, T., Roberts, R. G., 2004. Optical dating of Holocene sediments from a variety of geomorphic settings using single grains of quartz. Geomorphology 60 (3-4), 337-358.

Olley, J. M., Roberts, R. G., Murray, A., 1997. Disequilibria in the uranium decay series in sedimentary deposits at Allen's Cave, Nullarbor Plain, Australia: implications for dose rate determinations. Radiation Measurements 27 (2), 433-443.

Petraglia, M., Korisettar, R., Boivin, N., Clarkson, C., Ditchfield, P., Jones, S., Koshy, J., Lahr, M. M., Oppenheimer, C., Pyle, D., Roberts, R., Schwenninger, J.-L., Arnold, L., White, K., 2007. Middle Paleolithic Assemblages from the Indian Subcontinent Before and After the Toba Super-Eruption. Science 317 (5834), 114-116.

Roberts, R. G., Bird, M. I., Olley, J. M., Galbraith, R. F., Lawson, E. M., Laslett, G. M., Yoshida, H., Jones, R., Fullagar, R., Jacobsen, G. E., Hua, Q., 1998. Optical and radiocarbon dating at Jinmium rock shelter in northern Australia. Nature 393 (6683), 358-362.

Roberts, R. G., Galbraith, R. F., Olley, J. M., Yoshida, H., Laslett, G. M., 1999. Optical dating of single and multiple grains of quartz from Jinmium rock shelter, northern Australia: Part II, Results and Implications. Archaeometry 41 (2), 365-395.

Roberts, R. G., Galbraith, R. F., Yoshida, H., Laslett, G. M., Olley, J. M., 2000. Distinguishing dose populations in sediment mixtures; a test of single-grain optical dating procedures using mixtures of laboratory-dosed quartz. Radiation Measurements 32 (5-6), 459-465.

Sharma, G. R., Clark, J. D., 1983. Palaeoenvironments and Prehistory in the Middle Son Valley, Madhya Pradesh, north-central India. A. H. Wheeler and Co. Private Limited, Allahabad.

Story M., Roberts, R. G., Saidin, M., 2012. Astronomically calibrated $^{40}Ar/^{39}Ar$ age for the Toba supereruption and global synchronization of late Quaternary records. Proceedings of the National Academy of Sciences of USA, 109 (46), 18684-18688.

Thomsen, K. J., Murray, A. S., Jain, M., Bøtter-Jensen, L., 2008. Laboratory fading rates of various luminescence signals from feldspar-rich sediment extracts. Radiation Measurements 43 (9-10), 1474-1486.

Tiwari, M. P., Bhai, H. Y., 1997. Quaternary stratigraphy of the Narmada Valley. Geological Survey of India, Special Publication 46, 33-63.

Wallinga, J., Murray, A., Wintle, A., 2000. The single-aliquot regenerative-dose (SAR) protocol applied to coarse-grain feldspar. Radiation Measurements 32 (5-6), 529-533.

Williams, M. A. J., Ambrose, S. H., der Kaars, S. v., Ruehlemann, C., Chattopadhyaya, U., Pal, J., Chauhan, P. R., 2010. Reply to the comment on "Environmental impact of the 73 ka Toba super-eruption in South Asia" by M. A. J. Williams, S. H. Ambrose, S. van der Kaars, C. Ruehlemann,

U. Chattopadhyaya, J. Pal, P. R. Chauhan [Palaeogeography, Palaeoclimatology, Palaeoecology 284 (2009) 295-314]. Palaeogeography, Palaeoclimatology, Palaeoecology 296 (1-2), 204-211.

Williams, M. A. J., Ambrose, S. H., van der Kaars, S., Ruehlemann, C., Chattopadhyaya, U. C., Pal, J. N., Chauhan, P. R., 2009. Environmental impact of the 73 ka Toba super-eruption in South Asia. Palaeogeography, Palaeoclimatology, Palaeoecology 284 (3-4), 295-314.

Williams, M. A. J., Clarke, M. F., 1995. Quaternary geology and prehistoric environments in the Son and Belan Valleys, North Central India. Memoir - Geological Society of India 32, 282-308.

Williams, M. A. J., Pal, J. N., Jaiswal, M., Singhvi, A. K., 2006. River response to Quaternary climatic fluctuations: evidence from the Son and Belan valleys, north-central India. Quaternary Science Reviews 25 (19-20), 2619-2631.

Williams, M. A. J., Royce, K., 1982. Quaternary geology of the middle son valley, North Central India: Implications for prehistoric archaeology. Palaeogeography, Palaeoclimatology, Palaeoecology 38 (3-4), 139-162.

Figure Captions

Figure 1. (A) The study area. The locations of Palaeolithic, Mesolithic and Neolithic artefacts are after Sharma and Clark (1983). Sedimentary logs for sediments containing YTT ash at Ghoghara (B) and Khunteli (C) in the Middle Son Valley, Madhya Pradesh. A 50 cm stick is used for scale in the photos of the YTT ash unit in (B) and (C). A microphoto of a sample from the whitest (10YR 8/1) part of the YTT ash unit at Ghoghara (B) was taken using a digital camera mounted on a Leica MZ16A stereo microscope.

Figure 2. (A) WorldView-1 50 cm panchromatic imagery of the Rehi-Son confluence showing cliff sections where ash was observed in this study. The sites labelled 1, 2, 3 and 4 in (A) correspond to photographs 1, 2, 3 and 4, respectively, in (B). The lower ~4 cm of ash at the Ghoghara main section (photograph 1 in (B)) is thought to be primary ash (Gatti et al., 2011). The ash-rich units in photographs 2, 3 and 4 in (B) show evidence of re-working. The ash-rich unit in photo 2 shows evidence of mixing with silts, and the upper 10-20 cm of the sand underlying the ash-rich unit has lost its primary bedding and contains sharp discontinuities/fracture planes. This may record deformation of the sand unit below a cohesive ash-rich silt block, which has slumped into the river channel. The ash-rich units in photos 3 and 4 have diffusive/gradational contacts with the surrounding sediment (3, 4) indicative of fluvial transport and deposition. The geological hammer is 40 cm long, and the head is ~20 cm wide.

Figure 3. Radial plots of single-grain quartz OSL age distributions for samples GHO-2 (A), GHO-3 (B), KHUT-1 (C), and KHUT-4 (D). The $IRSL_{50}$ KF aliquot fading-corrected ages (open triangles) are superimposed on the quartz single-grain age distributions. (E) Single-grain $IRSL_{50}$ fading-corrected ages (black dots) and $IRSL_{50}$ fading-corrected aliquot ages (open triangles) from sample GHO-2 (data from Neudorf et al., 2012). A residual dose of 0.4 ± 0.1 Gy has been subtracted from the $IRSL_{50}$ data and the error on the residual dose has been propagated through into the error on the KF ages. Black solid lines are centred on the component ages identified by the Finite Mixture Model (FMM) of Roberts et al. (2000) for the quartz and KF single-grain data. The grey shaded band in each panel is centered on

the age calculated for the KF aliquot data using the Minimum Age Model (MAM) (Table 2). OD values are those calculated using CAM.

Figure 4. Single-grain quartz (A) and KF (B) D_e distributions for sample KHUT-10 collected from ~20 cm below the surface of a sandbar in the Son River channel. Multi-grain aliquot D_e distributions for KF grains from the same sample measured using the $IRSL_{50}$ (C) and the $pIRIR_{225}$ (D) signals. The grey shaded area should capture 95% of the points if they were statistically consistent (at 2σ) with 0 Gy in (A) (Galbraith et al., 1999). In plots (C) and (D), the grey bands are centered on the Minimum Age Model (MAM) estimates of D_e. Plots (A), (B) and (C) show that the OSL signal from quartz and the $IRSL_{50}$ signal from KF are generally well bleached, but that the $pIRIR_{225}$ signal has residual doses as high as 81 Gy (D).

Figure 5. Slumped river bank deposits, including fallen silty ash blocks adjacent to the Son River channel near the Ghoghara main section. During the monsoon season, these deposits are inundated by rising river water, washed into the river channel and transported downstream.

Figure 6. Radial plots of fading-corrected age distributions for samples GHO-2 (A), GHO-3 (B), KHUT-1 (C), and KHUT-4 (D). Solid circles are aliquots measured using the $IRSL_{50}$ signal and open triangles are aliquots measured using the $pIRIR_{225}$ signal. Residual doses of 0.4 ± 0.1 Gy and 6.6 ± 1.1 Gy have been subtracted from the $IRSL_{50}$ and $pIRIR_{225}$ data, respectively, and the uncertainties on the residual doses have been propagated through into the uncertainties on the ages.

Figure 7. Quartz and KF optical ages imply one of two possible scenarios: 1) the YTT ash sampled at Ghoghara and Khunteli has been reworked by fluvial processes and re-deposited either as fluvial silts (A) or as mobile, cohesive blocks (B), several thousand years after the Toba event; or 2) the YTT ash was deposited soon after the volcanic event ~74 ka ago, but the underlying sediments have since been eroded and replaced by younger, inset fluvial sediments (C).

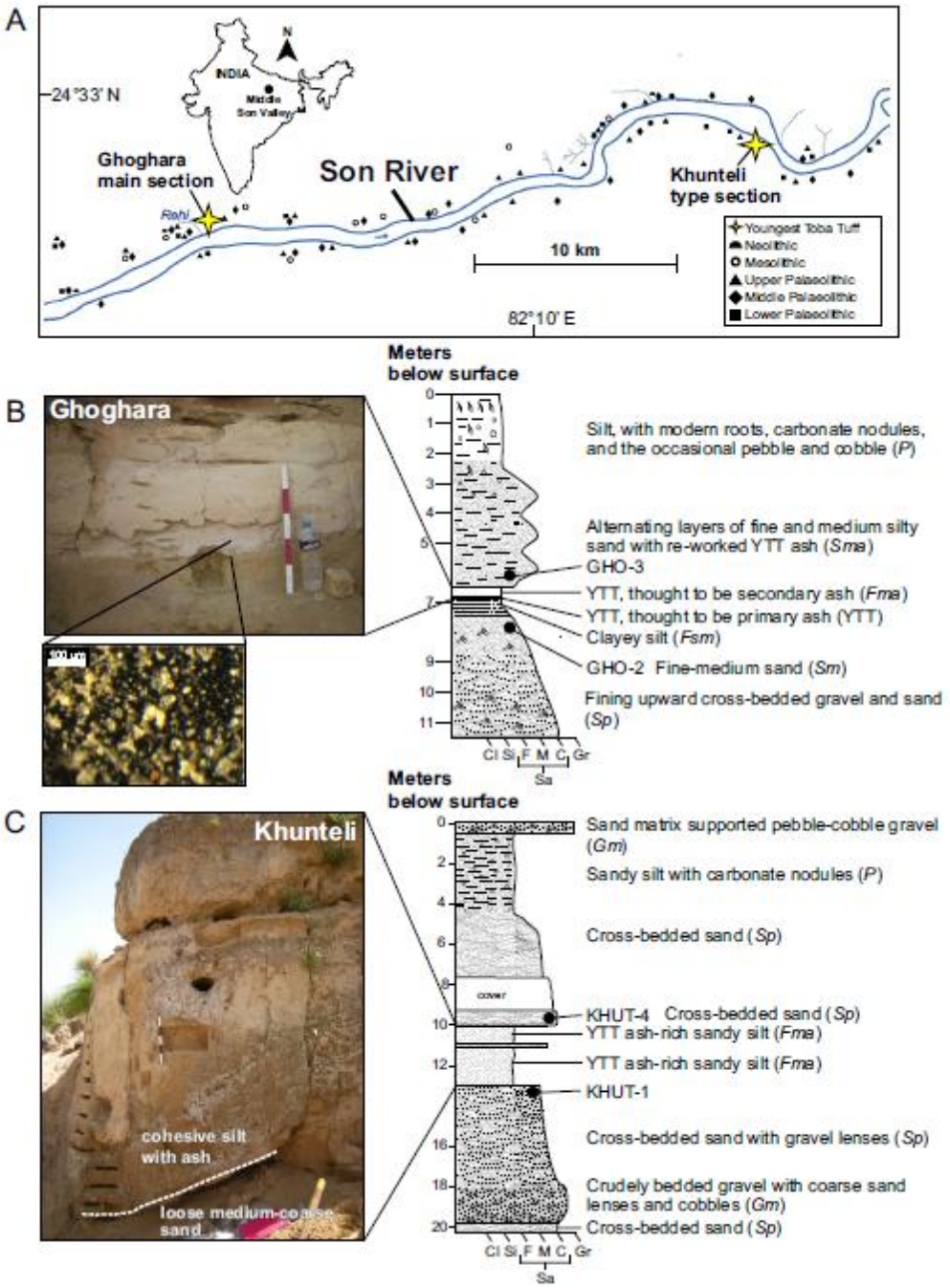

Figure 1

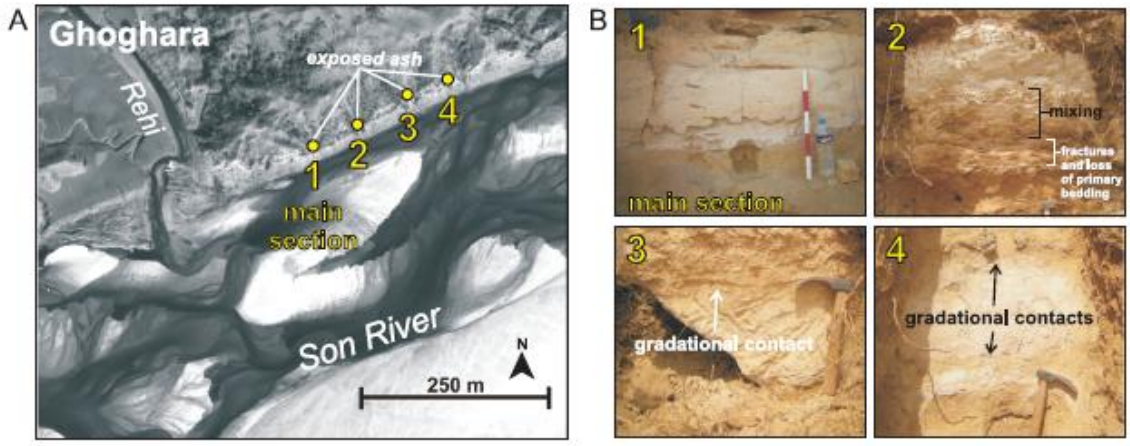

Figure 2

A GHO-2, quartz OD = 45 ± 2%

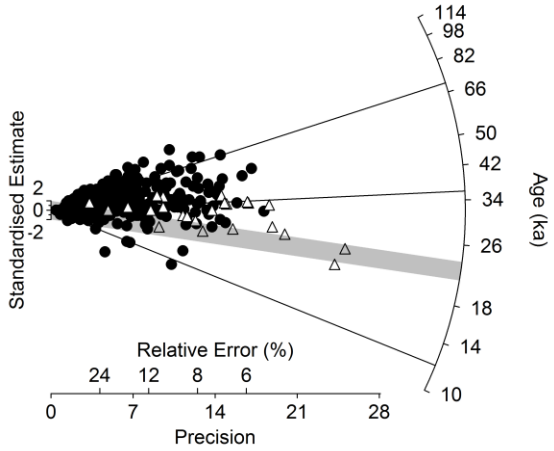

B GHO-3, quartz OD = 35 ± 2%

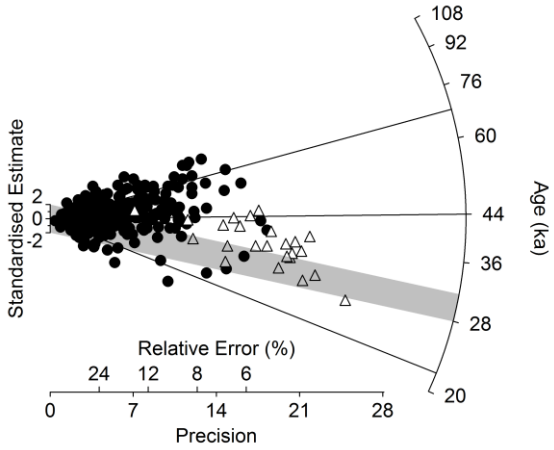

C KHUT-1, quartz OD = 37 ± 2%

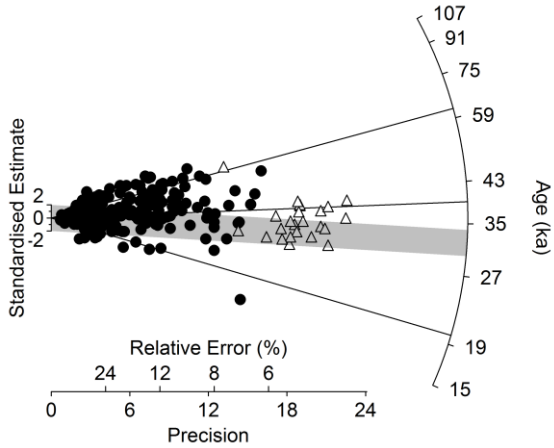

D KHUT-4, quartz OD = 38 ± 3%

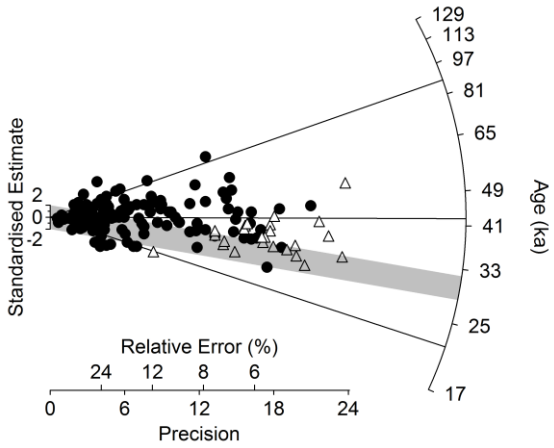

E GHO-2, KF (single-grain)
OD = 37.3 ± 1.5%

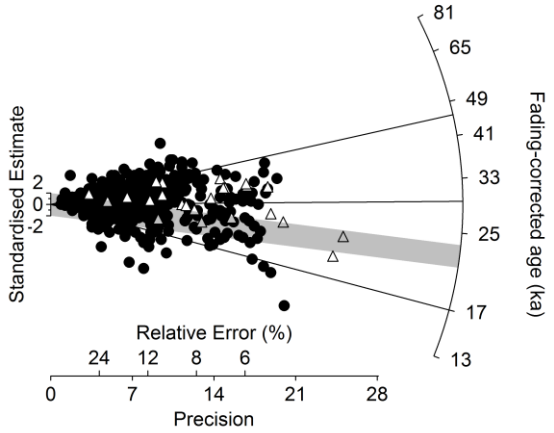

Figure 3

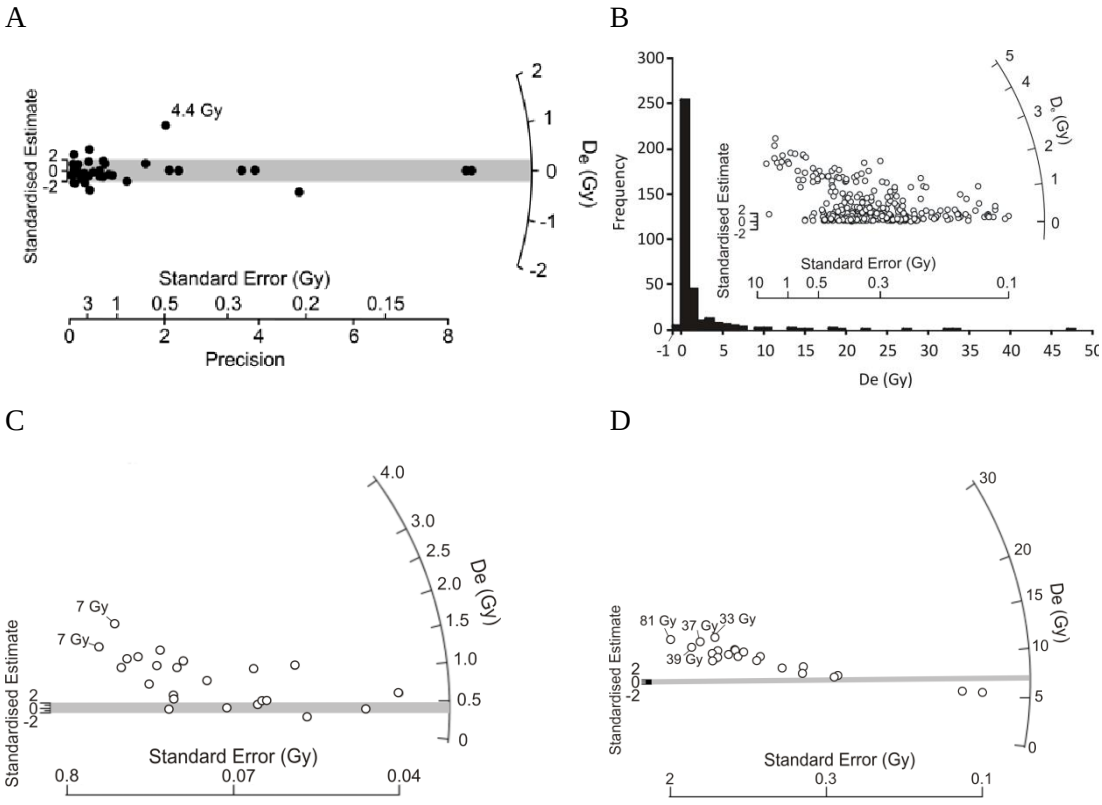

Figure 4

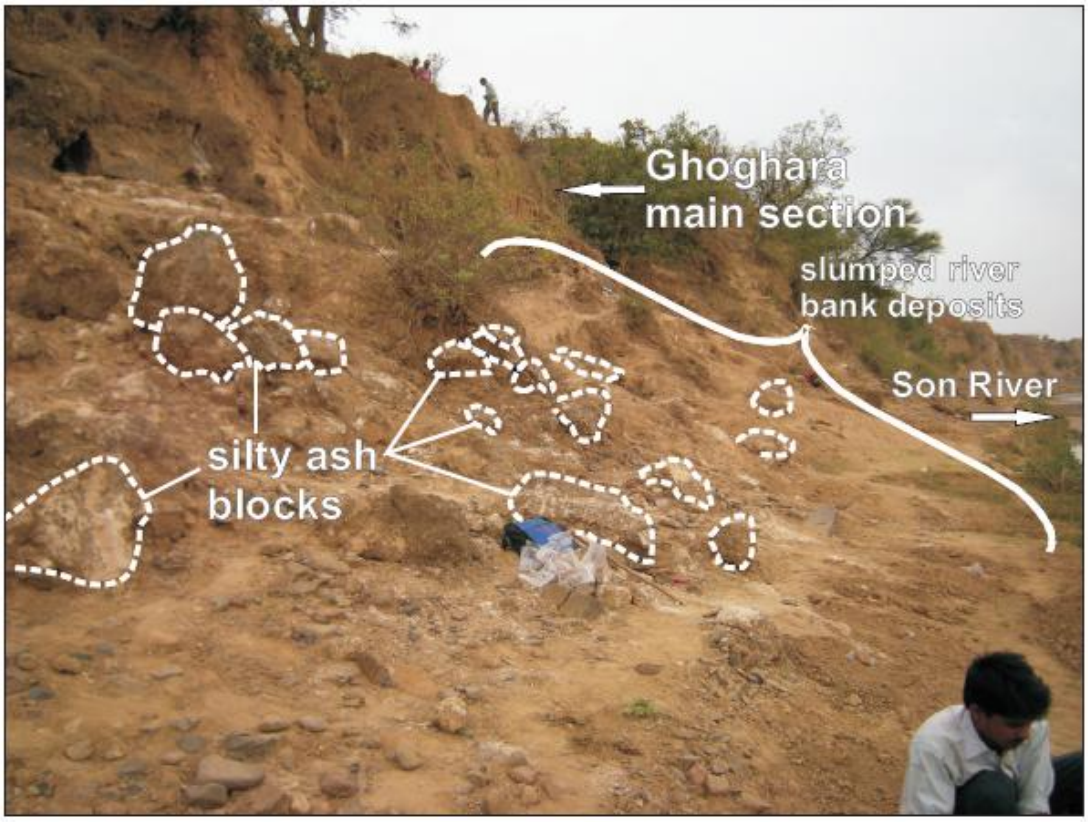

Figure 5

A GHO-2 – below ash

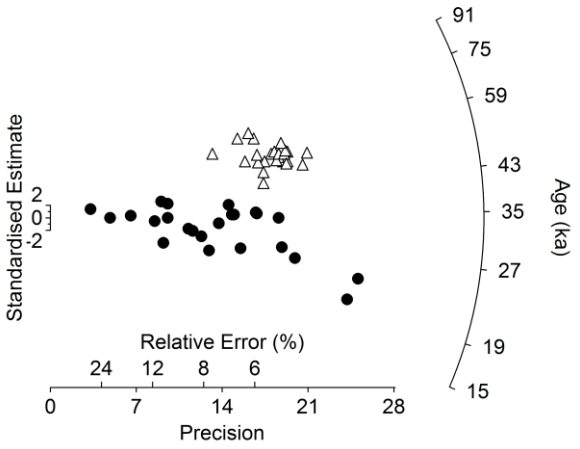

B GHO-3 – above ash

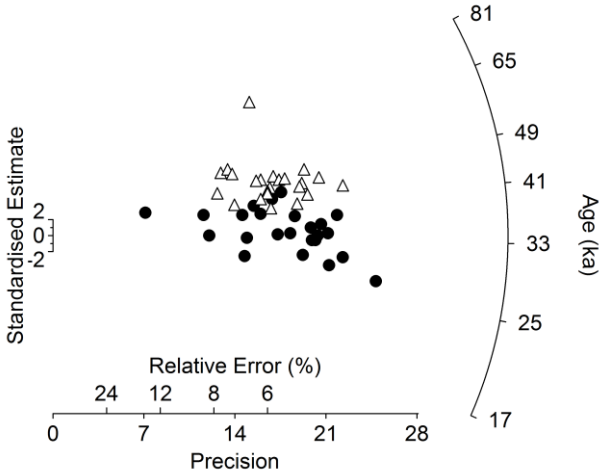

C KHUT-1 – below ash

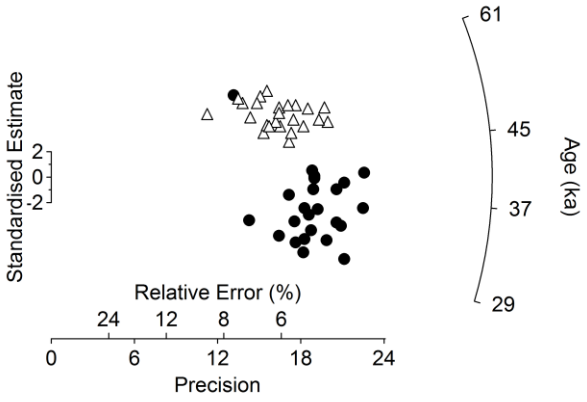

D KHUT4 – above ash

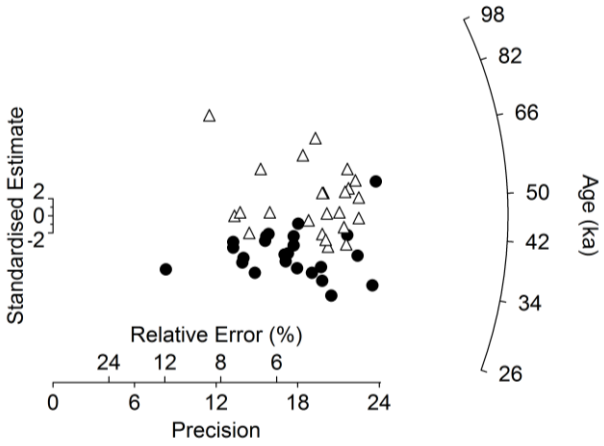

Figure 6

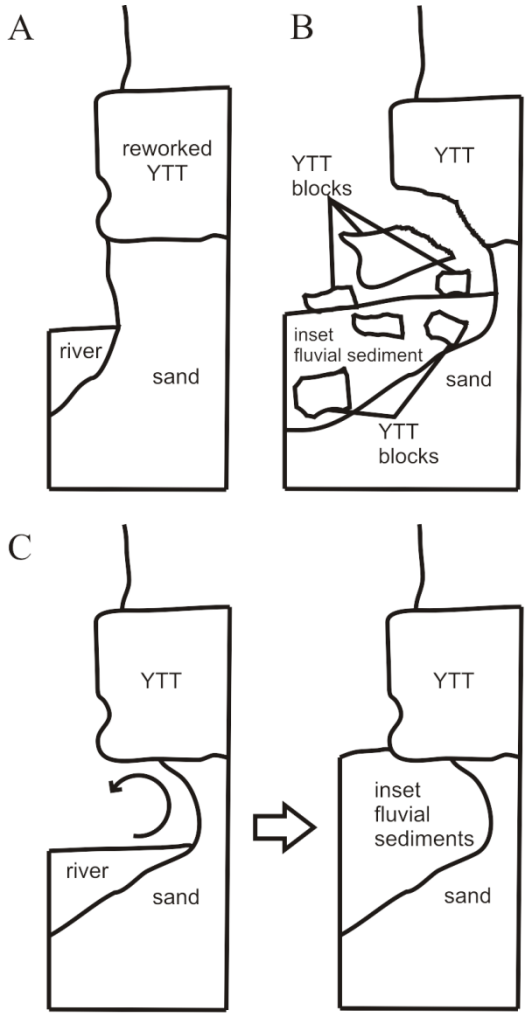

Figure 7

Table 1. Lithofacies codes (after Miall, 2006), descriptions and interpretations for sediments at the Ghoghara main section and the Khunteli Formation type-section.

Lithofacies	Code [a]	Colour	Description	Interpretation	Stratigraphic position	Geological section
Palaeosol	*P*	10YR 5/4	Silt with modern roots, carbonate nodules and the occasional pebble and cobble	Soil development in overbank fines	Above ash	Khunteli & Ghoghara
Gravel	*Gm*	–	Massive or crudely bedded sand matrix-supported pebble-cobble gravel	Gravel bar or bedform or lag deposit	Above and below ash (Khunteli)/ Below ash (Ghoghara)	Khunteli
Silty sand with reworked ash	*Sma*	10YR 7/4	Alternating layers of fine and medium silty sand with reworked ash and the occasional carbonate rhizolith	Overbank or floodplain fines	Above ash	Ghoghara
Ash-rich silt (secondary ash)	*Fma*	10YR 8/2	Ash-rich silt that is either massive or exhibits fine cross-lamination and ripples	Abandoned channel / pond / oxbow lake sediments on a floodplain	Ash	Khunteli & Ghoghara
Ash (primary ash?)	*YTT*	10YR 8/1	Massive with sharp undulating upper contact and sharp planar lower contact	Abandoned channel / pond / oxbow lake sediments on a floodplain	Ash	Ghoghara
Clayey silt	*Fsm*	10YR 7/6	Massive yellow clayey silt with gradational lower contact	Abandoned channel / pond / oxbow lake sediments on a floodplain	Below ash	Ghoghara
Fine-medium sand	*Sm*	10YR 7/4	Fine-medium silty sand with cross-laminae	Overbank or floodplain fines	Below ash	Ghoghara
Cross-bedded coarse sand and gravel	*Sp*	10YR 4/4	Micaceous coarse sand with planar cross-beds and gravel lenses	Sand bars or dunes in a channel	Below ash	Khunteli & Ghoghara

[a] The code scheme of Miall, (2006) where *P*, *G*, *S*, and *F* are symbols for palaeosol, gravel, sand and fine-grain sediments (silt/clay/mud), respectively. *m* = massive structure, *a* = contains ash, *s* = a dominant grain size of silt, and *p* = planar cross-beds.

Table 2. Single-grain (quartz and KF) FMM component ages and multi-grain KF $IRSL_{50}$ and $pIRIR_{225}$ D_e values, average fading rates and MAM and CAM ages for sediment samples from Ghoghara and Khunteli. Total dose rates are listed for both quartz and KF.

	Ghoghara main section			Khunteli type section		
Sample	**GHO-3 (above ash)**	**GHO-2 (below ash)**		**KHUT-4 (above ash)**	**KHUT-1 (below ash)**	**KHUT-10 (modern sample)**
			Single-grain FMM data [a]			
	Quartz	**Quartz**	**KF**	**Quartz**	**Quartz**	**Quartz**
N [b] (grains)	286	337	467	129	218	46
FMM component age 1 (ka)	22 ± 2 (8%)	12 ± 2 (3%)	17 ± 1 (17%)	22 ± 3 (15%)	20 ± 3 (8%)	
FMM component age 2 (ka)	44 ± 3 (54%)	36 ± 3 (57%)	30 ± 1 (52%)	43 ± 3 (75%)	39 ± 3 (52%)	–0.02 ± 0.12
FMM component age 3 (ka)	68 ± 5 (38%)	70 ± 5 (40%)	45 ± 2 (31%)	88 ± 15 (10%)	62 ± 5 (40%)	
OD (%) [c]	35 ± 2	45 ± 2	47 ± 2	38 ± 3	37 ± 2	2.5 ± 0.6
Total dose rates [d] (Gy/ka)	2.10 ± 0.07	1.45 ± 0.06	2.31 ± 0.07	0.85 ± 0.03	2.07 ± 0.07	
			$IRSL_{50}$ multi-grain KF data			
N [b] (aliquots)	24	24		24	24	
Average g-value [e] (%/decade)	3.1 ± 0.1	3.1 ± 0.1		3.5 ± 0.1	3.2 ± 0.1	
MAM fading-corrected De [f] (Gy) (OD in parantheses)	88.1 ± 4.9 (14 ± 2%)	51.6 ± 3.5 (20 ± 4%)		51.5 ± 1.7 (14 ± 3%)	93.5 ± 3.3 (15 ± 3%)	–0.4 ± 0.1 (92 ± 13%)
MAM age (ka) (assuming 5 ± 2% water content)	29.8 ± 1.8	22.3 ± 1.7		30.1 ± 1.2	31.9 ± 1.4	
MAM age (ka) (assuming 22 ± 7% water content)	33.6 ± 2.0	24.8 ± 1.8		32.7 ± 1.4	36.0 ± 1.6	
CAM age [g] (ka)	35.2 ± 1.6	30.2 ± 1.8		35.3 ± 1.6	35.3 ± 1.6	
			$pIRIR_{225}$ multi-grain KF data			
N [b] (aliquots)	24	24		24	24	
Average g-value [e](%/decade)	1.0 ± 0.1	1.7 ± 0.1		1.7 ± 0.1	1.2 ± 0.1	
MAM fading-corrected De [f] (Gy) (OD in parantheses)	141.9 ± 5.2 (16 ± 3%)	121.1 ± 13.0 (10 ± 2%)		72.5 ± 3.7 (22 ± 3%)	157.9 ± 3.7 (3 ± 2%)	6.6 ± 1.1 (64 ± 9%)
MAM age (ka) (assuming 5 ± 2% water content)	47.9 ± 2.1	52.4 ± 5.9		42.4 ± 2.4	53.9 ± 2.0	
MAM age (ka) (assuming 22 ± 7% water content)	54.7 ± 2.5	59.2 ± 6.6		47.0 ± 2.7	61.4 ± 2.3	
CAM age [g] (ka)	50.7 ± 2.5	53.4 ± 2.6		51.2 ± 3.0	53.8 ± 2.1	
Total dose rates for KF grains [d] (Gy/ka)	2.96 ± 0.08	2.31 ± 0.07		1.71 ± 0.04	2.93 ± 0.08	

[a] Quartz data obtained using the single-grain OSL dating procedures described in Haslam et al. (2011). Values in parentheses are the percentage of grains in each FMM component. All uncertainties are ± 1σ. The values shown for modern sample KHUT-10 are the overdispersion in D_e values and weighted mean D_e, both expressed in Gy.

[b] 'N' refers to the number of grains/aliquots with reliable D_e estimates.

[c] Overdispersion in D_e values as defined by Galbraith et al. (2005) and Galbraith and Roberts (2012).

[d] External dose rates were calculated from beta counting and *in situ* gamma spectrometry, using an assumed water content of 5 ± 2%. An assumed internal dose rate of 0.03 ± 0.01 Gy/ka was used for quartz, following Haslam et al. (2011) (see Supp. Mat. for explanation). Internal dose rates for KF grains and external dose rates for all samples are listed in Tables S5 and S6 of Supp. Mat..

[e] The weighted mean *g*-value (normalized to 2 days following Huntley and Lamothe, 2001) of all aliquots. Note that each aliquot was corrected for its own measured fading rate, not the mean fading rate listed in this table.

[f] The overdispersion in D_e values is shown in parentheses below each MAM estimate of D_e. Residual doses of 0.4 ± 0.1 Gy and 6.6 ± 0.1 Gy have been subtracted from the $IRSL_{50}$ and $pIRIR_{225}$ fading-corrected MAM D_e values, respectively, and the uncertainties on the MAM D_e values include a possible systematic error of ± 2% for beta-source calibration. All uncertainties are ± 1σ.

[g] CAM ages calculated assuming a 5 ± 2% water content.

Highlights

- Indian sediments containing Youngest Toba Tuff are dated using optical dating
- All age estimates post-date the ~74 ka Toba super-eruption
- The sediments contain fluvial and incompletely bleached slumped river bank deposits
- The tuff is an unreliable chronostratigraphic marker in palaeoenvironmental studies